frontiers | Frontiers in Earth Science

ORIGINAL RESEARCH
published: 28 June 2022
doi: 10.3389/feart.2022.921806

Application of the Grain-Based Rock-Eval Pyrolysis Method to Evaluate Hydrocarbon Generation, Expulsion, and Retention of Lacustrine Shale

Lingling Liao[1], *Yunpeng Wang*[2,3], *Chengsheng Chen*[2,3] *and Yinhua Pan*[1]*

[1]College of Environment and Resources, Guangxi Normal University, Guilin, China, [2]State Key Laboratory of Organic Geochemistry, Guangzhou Institute of Geochemistry, Chinese Academy of Sciences, Guangzhou, China, [3]University of Chinese Academy of Sciences, Beijing, China

OPEN ACCESS

Edited by:
Peng Cheng,
Guangzhou Institute of Geochemistry (CAS), China

Reviewed by:
Chao Yang,
Guangzhou Institute of Energy Conversion (CAS), China
Zhan-Wen Zhan,
Guangzhou Institute of Geochemistry (CAS), China
Qingtao Wang,
Guangzhou Institute of Energy Testing, China

***Correspondence:**
Yinhua Pan
panyh@mailbox.gxnu.edu.cn

Specialty section:
This article was submitted to Geochemistry, a section of the journal Frontiers in Earth Science

Received: 16 April 2022
Accepted: 10 May 2022
Published: 28 June 2022

Citation:
Liao L, Wang Y, Chen C and Pan Y (2022) Application of the Grain-Based Rock-Eval Pyrolysis Method to Evaluate Hydrocarbon Generation, Expulsion, and Retention of Lacustrine Shale. Front. Earth Sci. 10:921806. doi: 10.3389/feart.2022.921806

The study on hydrocarbon generation, expulsion, and retention of shale is becoming more and more important as the exploration of unconventional oil and gas worldwide. There are multiple sets of lacustrine shales in the eastern area of China, which show a great potential for shale oil/gas exploration. In this study, a grain-based Rock-Eval pyrolysis method was conducted on three sets of lacustrine shales, including the Nenjiang shale, Shahejie shale, and Maoming oil shale, to evaluate the hydrocarbon generation, expulsion, and retention. For comparison, pyrolysis of kerogen from the three shale samples was also carried out under the same experimental conditions. The Maoming oil shale showed a slightly broader distribution of activation energies than the Nenjiang and Shahejie shales, while the Nenjiang shale showed higher dominant activation energy than the Shahejie shale and the Maoming oil shale. At laboratory heating rates (5–25°C/min), the corresponding temperature to the maximum hydrocarbon generating rate of shale grains was collectively higher than that of their kerogen, especially for the Nenjiang and Shahejie shales, which implies a lagging effect during the hydrocarbon generation and expulsion process for the shales. By calculating the differences in hydrocarbon yields between shale grain and kerogen samples, the content and proportion of the retained hydrocarbons were measured at different maturation stages. The results showed that the Nenjiang shale from the Songliao Basin has the strongest retention ability but the weakest expulsion ability, whereas the Shahejie shale from the Dongying Depression has the strongest expulsion ability but the weakest retention ability among the three samples. Moreover, it is found that the pore structure of lacustrine shales is likely the principal factor controlling the hydrocarbon retention ability/capacity. This study is expected to provide a geochemical quantitative basis for evaluating hydrocarbon generation, expulsion, and retention of shale.

Keywords: grain-based, Rock-Eval pyrolysis, kinetic, geological implication, lacustrine shale

INTRODUCTION

The increased demand for fossil energy and continuous depletion of conventional oil and gas resources have raised great attention to unconventional energy resources in the recent decade (Bowker, 2007; Jarvie et al., 2007; Tang et al., 2014; Wang et al., 2015; Jia, 2020). Inspired by the great success of shale gas exploration and development in North America, many countries such as China, India, Poland, South Africa, Australia, Ukraine, and United Kingdom are urgent to evaluate their shale gas resources to cope with the growing energy demand (Zou et al., 2010; Badics and Vető, 2012; Horsfield and Schulz, 2012; Ji et al., 2014; Wang et al., 2014; Wang et al., 2015; Cheng et al., 2019; Cheng et al., 2022).

Shales, the main reservoir for oil and gas resources, have been the major subject of the unconventional oil/gas study (Xie et al., 2016). Organic-rich and low-thermal mature lacustrine shales that are widely distributed in China have been regarded as the main target rocks for shale oil resources, especially for the light shale oils with high recovery efficiency (Yang et al., 2005; Hanson et al., 2007; Hu et al., 2008; Liu et al., 2010; Li et al., 2012; Lamei et al., 2013; Tang et al., 2014; Peng and Jia, 2021). Some breakthroughs have been made in continental shales in China, especially marked by the success of well Liuping 177 drilled in Zhangjiatan shale of the Triassic Yanchang Formation in Ordos Basin (Guo et al., 2014; Ji et al., 2014; Yu et al., 2017). In recent years, numerous studies have been conducted on unconventional shale oil resources, and many of them are devoted to the resource potential assessment of lacustrine shales (e.g., Wang et al., 2015; Wang et al., 2019; Li et al., 2022; Wang et al., 2022). Therefore, the resource assessment of shale gas/oil is a key problem in the exploration of unconventional oil/gas (Cheng et al., 2017, 2018; Jin et al., 2021). The methodology of lithology, organic geochemistry, or petroleum geology has been applied in the assessment of shale oil potential and its controlling factors (Li et al., 2020, 2021). For example, Li et al. (2020) studied the fine-grained sedimentary rocks of the Eocene Shahejie Formation by combining mineralogy and organic geochemistry and showed that complex lithologies of the rocks control their shale oil potential.

Our previous work (Liao et al., 2018) suggested that grain-based Rock-Eval pyrolysis is an efficient method to evaluate the evolution of hydrocarbon generation, expulsion, and retention. It is suggested that the hydrocarbon yield of kerogen represents the total content of hydrocarbon generation of organic matter, while the hydrocarbon yield of shale grains represents the content of hydrocarbon expulsion. Hence, the retention content of grains is recognized as the difference between the total content of hydrocarbon generation of kerogen and the content of hydrocarbon expulsion of grains (Cornford et al., 1998). This may provide an efficient method for evaluating the characteristics of hydrocarbon generation, expulsion, and retention of shales by the grain-based Rock-Eval pyrolysis method. In the present study, we investigated shale grain and kerogen samples derived from three low mature lacustrine shale samples from the Songliao Basin, the Dongying Depression, and the Maoming Basin. The Rock-Eval pyrolysis results at different heating rates were calculated to reveal the kinetic parameters, and thus extrapolated to geological conditions. The evolutions of hydrocarbon generation, expulsion, and retention characteristics of the lacustrine shales, as well as the main factors controlling hydrocarbon expulsion and retention, were further explored.

SAMPLES AND EXPERIMENTS

Samples

Overall three organic-rich lacustrine shale samples from China were selected for kinetic analysis. Nenjiang (NJZ) is an outcrop sample of the Late Cretaceous Nenjiang Formation (K_2n_2), collected from the Songliao Basin. Shahejie (SHJ) belongs to the Lower Paleocene Shahejie Formation (Es_1), collected from the Dongying Depression of Bohai Bay Basin. Maoming (MM) is an outcrop oil shale of Eocene to the Oligocene Youganguo Formation ($E_{2\text{-}3}y$) from the Maoming Basin (Brassell et al., 1986). The geochemical data for the source rocks are presented in **Table 1**. The samples were prepared into two forms including grains (diameter of 4 mm) and kerogen for Rock-Eval temperature-programmed pyrolysis. Details on sample preparation can be found in our previous work (Liao et al., 2016, 2018). In brief, samples were taken from a single rock using a micro-drilling method along a vertical direction to avoid or minimize the heterogeneity across different lamellar layers.

The results of hydrogen index (HI) versus T_{max} from NJZ shale, SHJ shale, and MM oil shale collected from different basins are plotted in the diagram to determine the kerogen type and maturity by the method of Mukhopadhyay et al. (1995). As is

TABLE 1 | Geochemical data for samples used in the pyrolysis study.

Sample	Location	Form	S_1 (mg/g)	S_2 (mg/g)	HI (mg/g TOC)	T_{max} (°C)	TOC (%)	R_o (%)	Kerogen type
NJZ	Songliao Basin	Grain	0.11	10.29	415	433	2.48	0.52	I
		Kerogen	8.65	414.24	659	432	62.86		
SHJ	Bohai Bay Basin	Grain	0.32	15.35	564	426	2.72	0.45	II
		Kerogen	8.19	229.68	589	421	39.02		
MM	Maoming Basin	Grain	1.85	162.95	564	429	28.88	0.43	I
		Kerogen	2.92	255.84	654	427	39.1		

TOC: total organic carbon; S_1: free hydrocarbons; S_2: pyrolysis of hydrocarbons; T_{max}: pyrolysis temperature at maximum hydrocarbon generation; R_o: vitrinite reflectance (%).

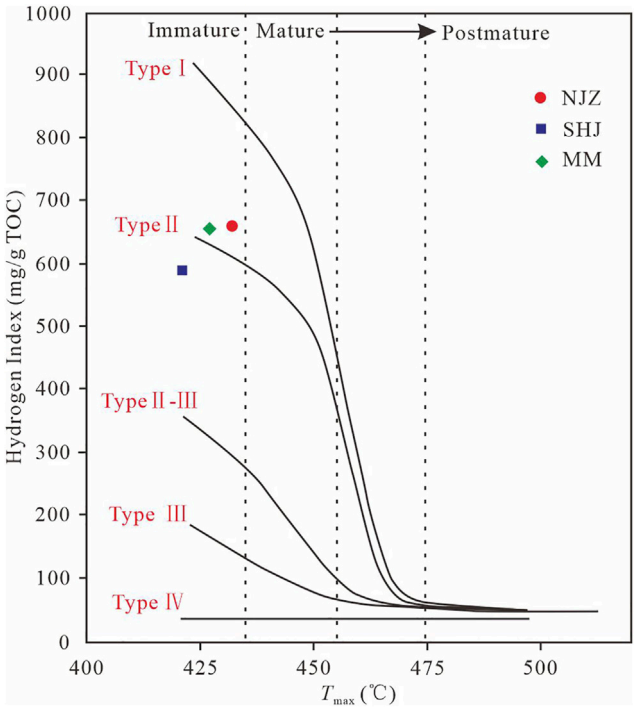

FIGURE 1 | Hydrogen index (HI) plotted versus T_{max} values modified from Shalaby et al. (2011).

shown in **Figure 1**, three samples are generally plotted in the immature zone comprising type I and type II kerogen. NJZ shale and MM oil shale were assigned relatively higher HI of type I kerogen while SHJ shale was the lower HI area of type II kerogen. The total organic carbon (TOC) analysis shows high TOC values for the shale samples, with the values being 2.48, 2.72, and 28.88% for NJZ, SHJ, and MM shales. The maturity rates (%R_o) for the three shale samples are 0.52, 0.45, and 0.43%, respectively (**Table 1**). Therefore, the shale samples with higher TOC contents and lower maturities are suitable for in-laboratory simulation.

Rock-Eval Temperature-Programmed Pyrolysis

Rock-Eval temperature-programmed pyrolysis was performed using an Rock-Eval 6 instrument. Samples were pyrolyzed at a temperature range of 300–650°C with heating rates of 5°C/min, 15°C/min, and 25°C/min, respectively. Pyrolysis parameters including TOC, S_1, S_2, and T_{max} (temperature of maximum pyrolysis yield) were measured. HI was calculated by the formula $S_2 \times 100$/TOC as described by Espitalié et al. (1977), Peters and Cassa (1994), and Shalaby et al. (2011). The experiment procedures have been described in detail by Liao et al. (2018). Based on the Rock-Eval pyrolysis results, the kinetic parameters were further calculated by the method of Liao et al. (2018). In brief, kinetic parameters (discrete activation energy and frequency factor) for grains and kerogen were calculated by Kinetic 2000 software. Assuming parallel first-order reactions with a single frequency factor and activation energies, different heating rates were used to achieve optimal values. Optimization results in a best fit for calculated curves and measured curves (Han et al., 2014). In addition, the activation energy obeys the discrete distributed model (Miura, 1995).

RESULTS AND DISCUSSION

Characteristics of Hydrocarbon Generation and Expulsion

Figures 2–4 show the hydrocarbon generation rates and yields of grains and kerogen from NJZ shale, SHJ shale, and MM oil shale as a function of pyrolysis temperature at each heating rate, respectively. The pyrolysis characteristics of grains and kerogen are similar to those of Pingliang marine shale and Yanchang lacustrine shale in Liao et al. (2018), all showing that the total amount of hydrocarbon generation is identical regardless of the pyrolysis heating rate for each sample (Behar et al., 1992). **Figure 5** shows the hydrocarbon generating rates of grains and kerogen for each sample at different heating rates. It is apparent that the corresponding pyrolysis temperatures to the maximum hydrocarbon generating rates for grain samples are collectively higher than those for corresponding kerogen samples, that is, the temperatures of shale grains are respectively 7°C, 6, and 9°C higher than its kerogen for NJZ shale at the heating rates of 5°C/min, 15°C/min, and 25°C/min while 8°C, 8, and 9°C for SHJ shale and 5°C, 2 and 3°C for MM oil shale. It is generally proposed that kerogen pyrolysis can represent the hydrocarbon generation of pure organic matter, while grain pyrolysis can represent both generation and expulsion processes of source rock (Inan et al., 1998; Liao et al., 2018). As a consequence, the generated hydrocarbons cannot be expelled out in time which gives rise to a lagging effect (Inan et al., 1998). The results also show that both NJZ shale and SHJ shale show a larger lagging effect (i.e. slower hydrocarbon expulsion) than MM oil shale at different heating rates. This indicates that the lagging effect varies among different shale samples, possibly due to the differences in mineralogical composition and organic content of the shales.

There are significant differences in the hydrocarbon yields of grains and kerogen for the shale samples at various heating rates (**Figure 6**). Taking 15°C/min as an example, the differences in total yield between grains and kerogen are 267 mg/g TOC for NJZ shale, 67 mg/g TOC for SHJ shale, and 134 mg/g TOC for MM oil shale, indicating distinct retention/adsorption capability for the shales. The NJZ shale shows the strongest retention capability among the three shale samples, followed by MM oil shale, and SHJ shale is the weakest.

Activation Energy Distributions

Figure 7; **Table 2** show the activation energy distributions as well as the frequency factor (A) for grains and kerogen from NJZ, SHJ, and MM shales, respectively. The kinetic calculation was shared with a given frequency factor $A = 1.98E{\times}10^{12}$ s^{-1} (Wang et al., 2006; Han et al., 2014). For NJZ shale, the discrete activation energy distribution ranges from 38 to 60 kcal/mol and

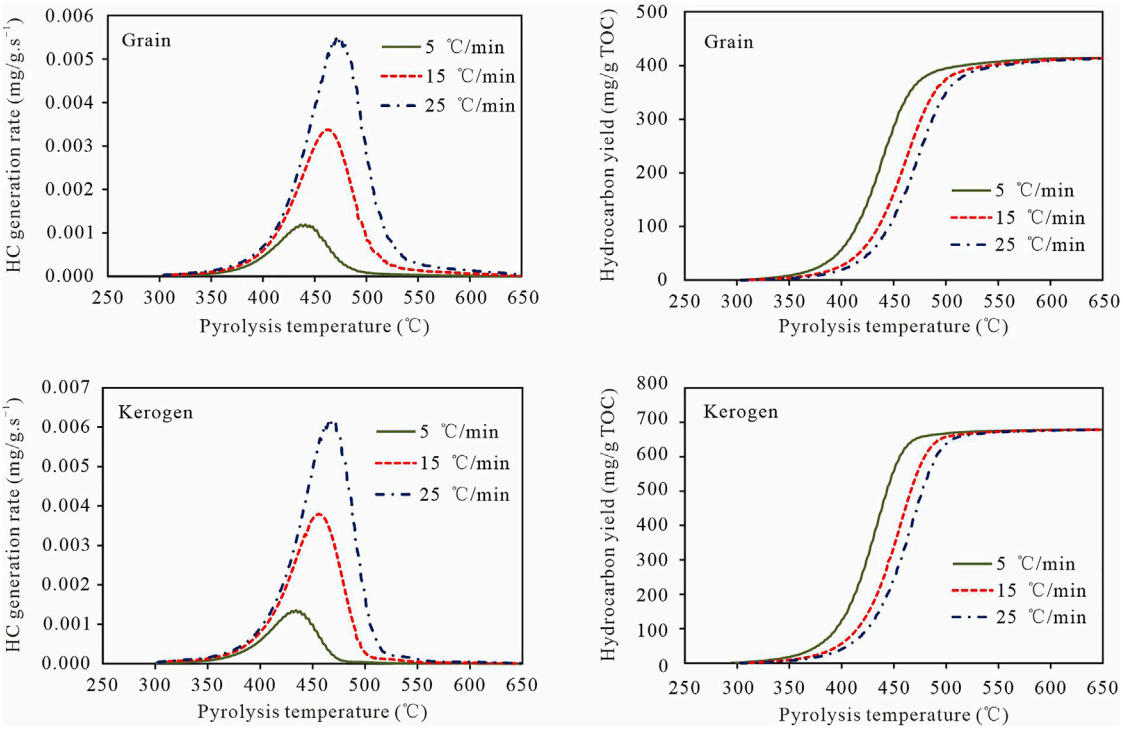

FIGURE 2 | Hydrocarbon (HC)-generating rates and hydrocarbon yield of grain and kerogen from NJZ shale as a function of pyrolysis temperature at different heating rates.

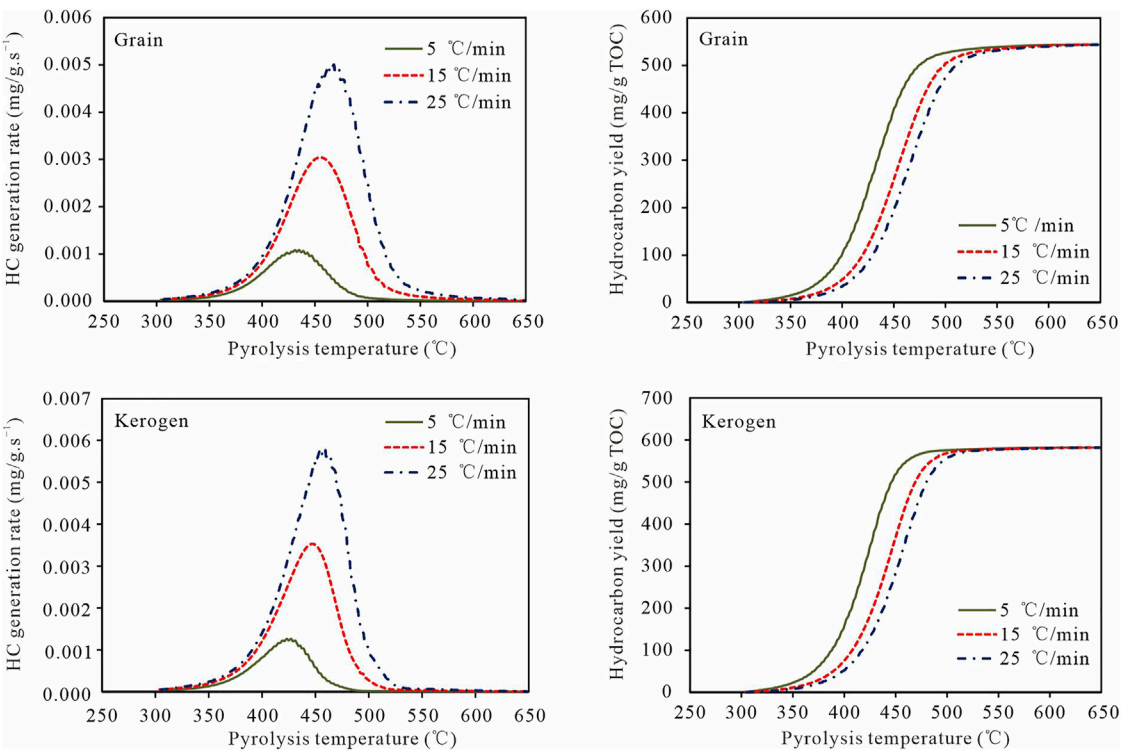

FIGURE 3 | Hydrocarbon (HC)-generating rates and hydrocarbon yield of grain and kerogen from SHJ shale as a function of pyrolysis temperature at different heating rates.

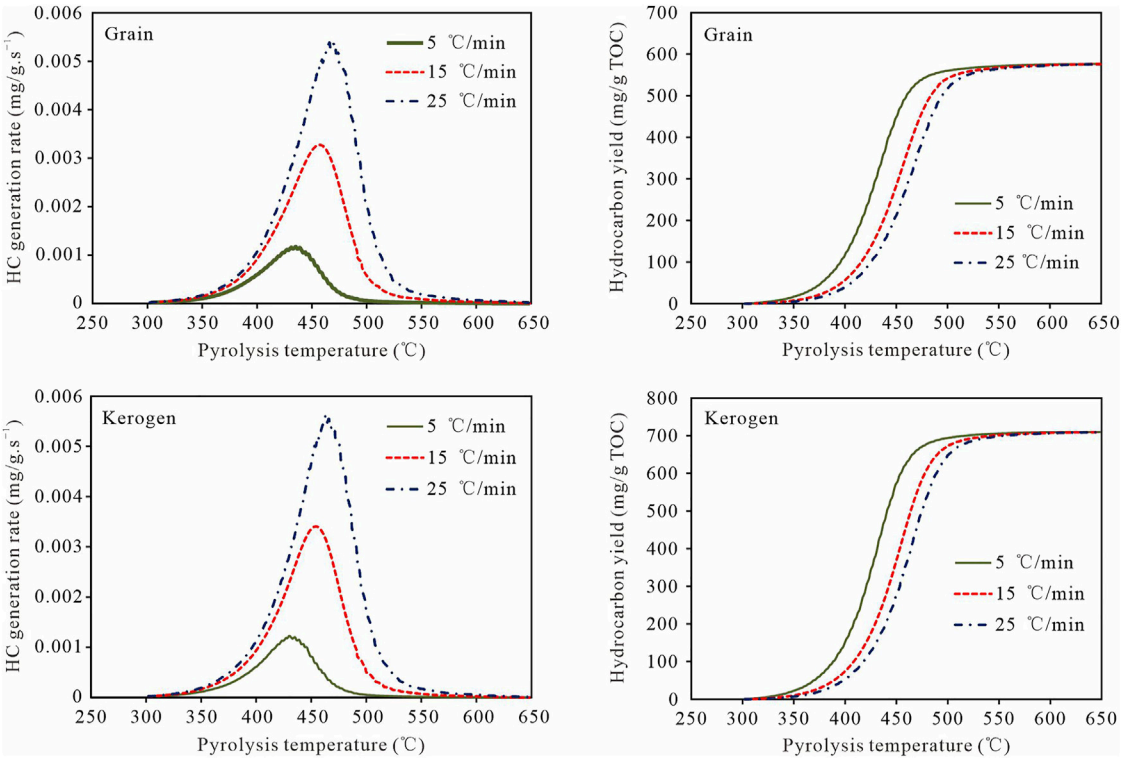

FIGURE 4 | Hydrocarbon (HC)-generating rates and hydrocarbon yield of grain and kerogen from MM oil shale as a function of pyrolysis temperature at different heating rates.

38–59 kcal/mol for grains and kerogen, respectively. In addition, the grains and kerogen exhibit the same dominant activation energy (E_{max}) of 48 kcal/mol. The discrete activation energy distributions of SHJ shale display an identical range of 38–58 kcal/mol for grains and kerogen, with their E_{max} values being 48 kcal/mol and 47 kcal/mol, respectively. Similarly, the discrete activation energy distributions for grains and kerogen of MM oil shale are in the range of 38–61 kcal/mol and 38–58 kcal/mol, and E_{max} values are 48 kcal/mol and 47 kcal/mol, respectively. In comparison, NJZ kerogen show relatively higher E_{max}, suggesting a higher hydrocarbon generation threshold relative to SHJ and MM kerogen. This implies that SHJ shale and MM oil shale need relatively lower energy to commence hydrocarbon generation but relatively higher energy for hydrocarbon expulsion, while NJZ shale requires higher energy for both processes.

Geological Implications

The kinetic parameters were extrapolated to a "hypothetical" geological heating rate of 3°C/Ma (Schenk et al., 1997). **Figure 8**; **Table 3** show the conversion rate versus geological temperature and maturity (%R_o) for grains and kerogen of NJZ shale, SHJ shale, and MM oil shale. The corresponding maturity (geological temperature) rates to the main hydrocarbon generation period (MHGP) for the NJZ grain and kerogen samples are in the range of 0.63–0.91% (110–145°C) and 0.61–0.80% (108–134°C), respectively. Similarly, the corresponding maturity rates (geological temperature) to the MHGP for SHJ grain and kerogen samples are 0.58–0.88% (106–142°C) and 0.54–0.77% (103–131°C), while 0.55–0.86% (104–140°C) and 0.55–0.84% (104–138°C) for MM oil shale. NJZ grains and kerogen exhibit higher maturities and geological temperatures than those for SHJ and MM shales, which is indicative of a later hydrocarbon generation and expulsion. Furthermore, MM grains and kerogen show the broadest range of maturity and geological temperature among these samples, while those for both NJZ and SHJ shales become progressively narrower. This may indicate that MM oil shale enjoys the longest hydrocarbon generation and expulsion period.

Figure 9 shows the hydrocarbon expulsion rates for grains and kerogen of three samples at a geological heating rate of 3°C/Ma. The grains and kerogen of all shale samples show a typical single hydrocarbon expulsion peak with the increase of temperature. The corresponding maturities (geological temperatures) to the maximum hydrocarbon expulsion rates for the NJZ grain and kerogen samples are both 0.76% (130°C), while those for the SHJ grain and kerogen samples are, respectively, 0.75% (129°C) and 0.74% (127°C) and for the MM grain and kerogen samples both are 0.74% (127°C). In comparison to the SHJ shale and the MM oil shale, the NJZ shale shows a relatively higher maturity when reaching the maximum hydrocarbon expulsion rate, which suggests its higher threshold for hydrocarbon expulsion.

With regard to hydrocarbon retention of shale, the calculation method for hydrocarbon retention content and retention

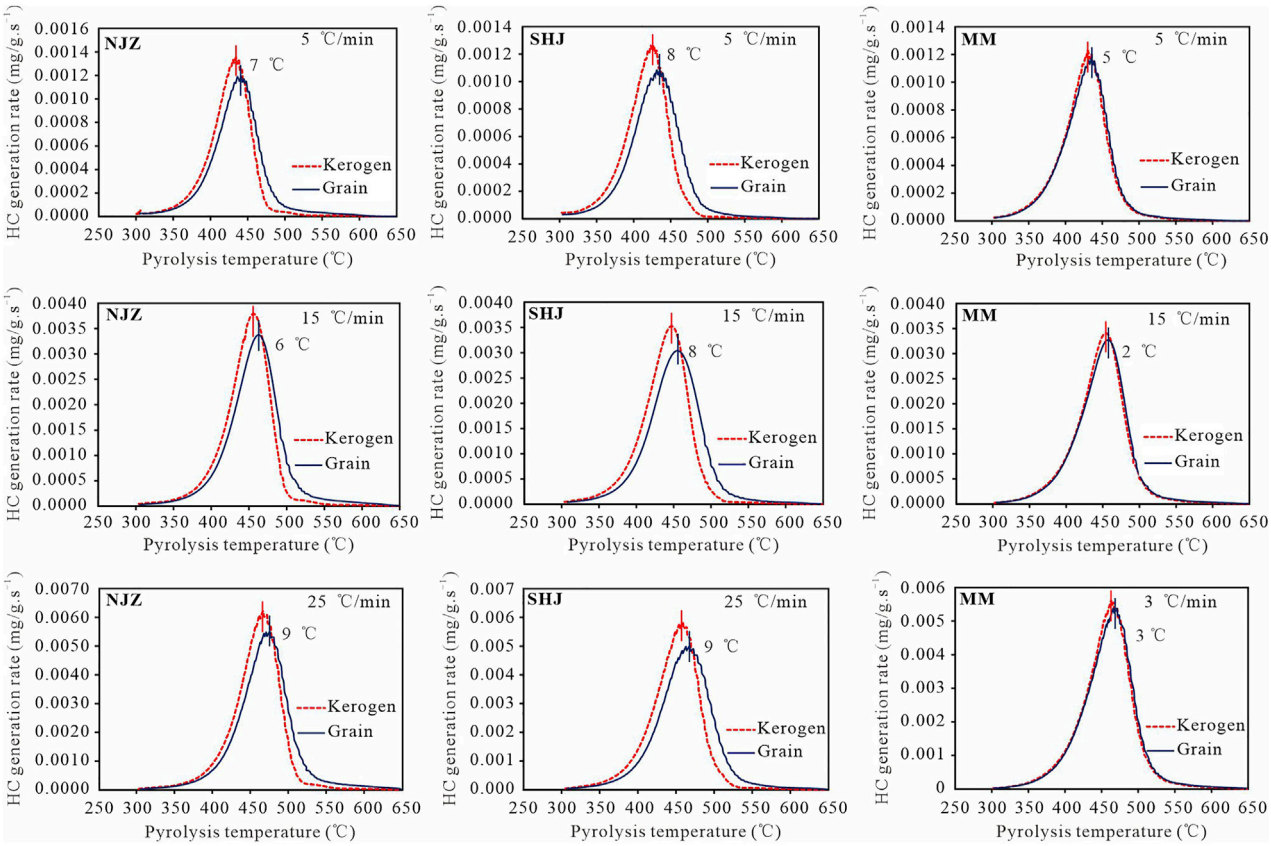

FIGURE 5 | Hydrocarbon (HC)-generating rate of grain and kerogen for NJZ shale, SHJ shale, and MM oil shale at the heating rates of 5°C/min, 15°C/min, and 25°C/min.

proportion has been described in detail by Liao et al. (2018). Also, a detailed discussion of hydrocarbon generation stages (i.e. stage I and stage II) is presented in our previous work (Liao et al., 2018), in which stage I represents the stage after the peak of hydrocarbon generation and stage II represents the stage after second cracking.

Figure 10; **Table 4** show the evolution of hydrocarbon generation, expulsion, and retention for three samples at a geological heating rate of 3°C/Ma. At a stage, I (R_o = 1%), the hydrocarbon yields for NJZ grains and kerogen are 384.71 mg/g TOC and 659.65 mg/g TOC, respectively. Similarly, the hydrocarbon yields for SHJ grains and kerogen are 515.61 mg/g TOC and 573.58 mg/g TOC while those for MM oil shale are 551.08 mg/g TOC and 683.50 mg/g TOC, respectively. As the difference in hydrocarbon yields between shale grain and kerogen samples is recognized as the hydrocarbon retention content of the shales (Cornford et al., 1998), the content and proportion of the retained hydrocarbons could be calculated based on the hydrocarbon yields. The hydrocarbon retention content and the retention proportion for NJZ shale are 274.94 mg/g TOC and 41.68%, while 57.97 mg/g TOC and 10.11% for SHJ shale and 132.42 mg/g TOC and 19.37% for MM oil shale, respectively. Similarly, at stage II (R_o = 3%), the retention content and proportion for NJZ shale are 264.82 mg/g TOC and 39.01%, while 38.03 mg/g TOC and 6.53% for SHJ shale and 133.26 mg/g TOC and 18.78% for MM oil shale, respectively. By comparison of the hydrocarbon retention data, it offers us an opportunity to estimate the retention ability of shale samples. Taking Yanchang Formation (YC-L) into consideration (Liao et al., 2018), NJZ shale has the highest retention content among these shale samples while those for MM oil shale, YC-L shale, and SHJ shale become progressively lower at both stage I and stage II. This may suggest that NJZ shale from the Songliao Basin is of the strongest retention ability but of the weakest expulsion ability for prevalent continental shales in China. However, SHJ shale from the Dongying Depression has stronger hydrocarbon expulsion ability but weaker hydrocarbon retention ability.

Analysis of Influencing Factors of Hydrocarbon Expulsion and Retention

Pore structure parameters, such as pore volume, special surface area, porosity, permeability, and pore size diameter, are available for the evaluation of natural gas reservoirs (Chalmers and Bustin, 2007; Ross and Bustin, 2009; Chalmers et al., 2012; Mastalerz et al., 2012; Zhang et al., 2017a, 2017b). For example, many previous studies suggested that the abundance of pores in shales is mainly controlled by the compositions of minerals and organic matter (Loucks et al., 2012; Ma et al., 2015; Xiong et al., 2015; Li

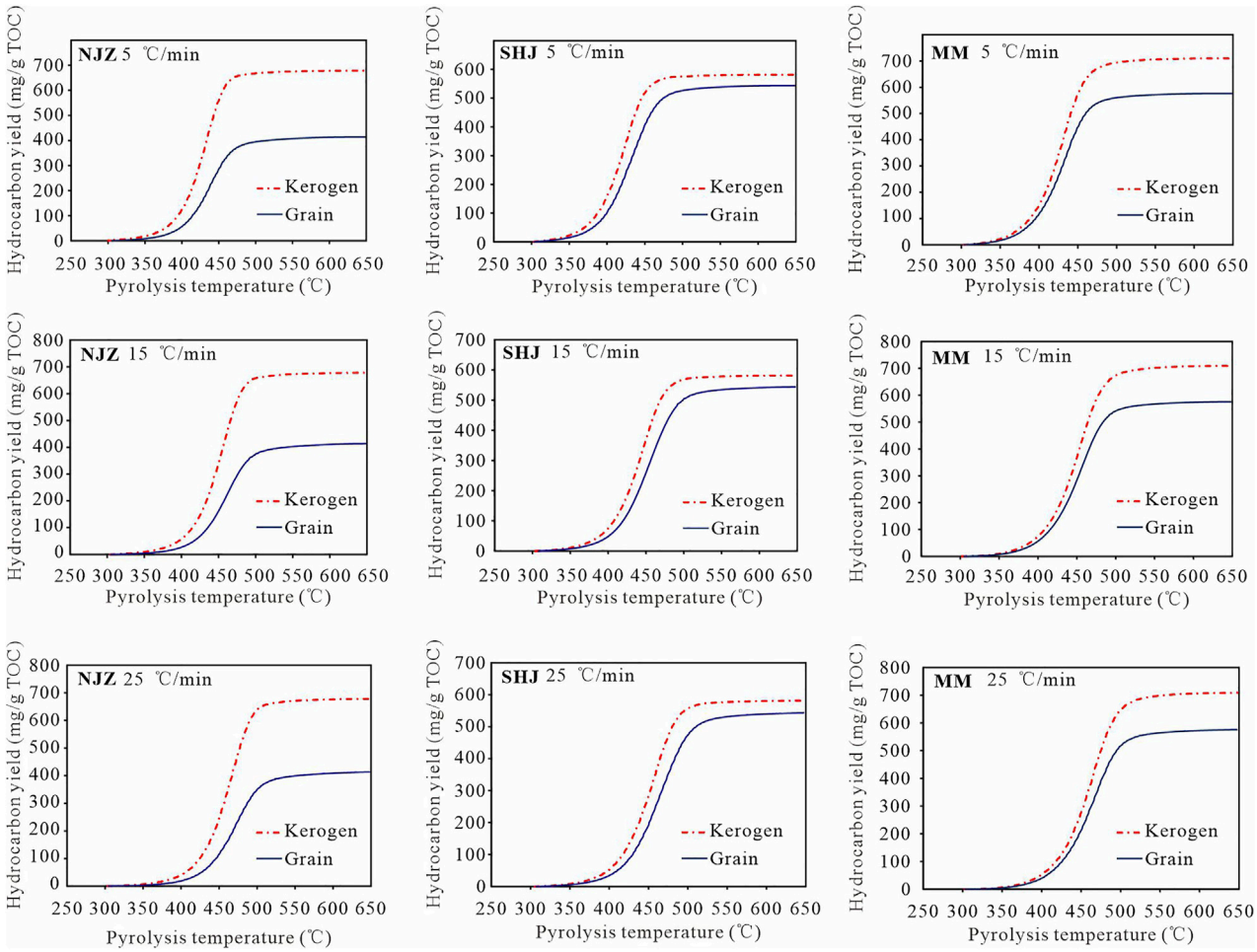

FIGURE 6 | Hydrocarbon yield of grain and kerogen for NJZ shale, SHJ shale, and MM oil shale at the heating rates of 5°C/min, 15°C/min, and 25°C/min.

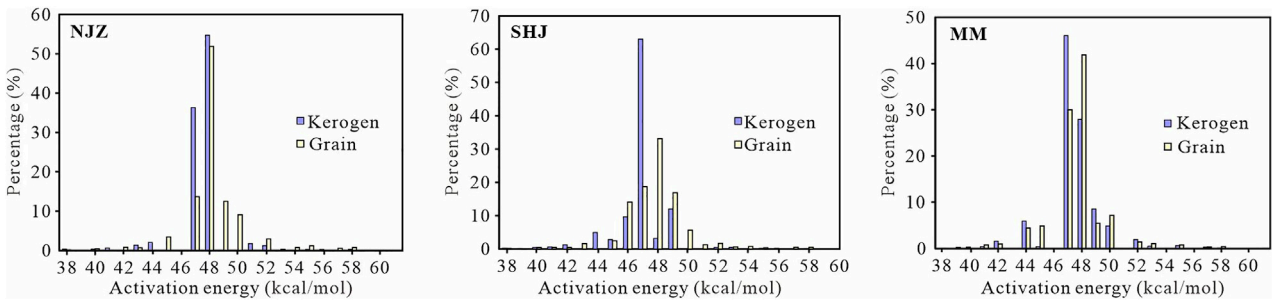

FIGURE 7 | Distribution of activation energies with the universal frequency factor **(A)** for grain and kerogen from NJZ shale, SHJ shale, and MM oil shale.

et al., 2016; Han et al., 2019). Therefore, X-ray diffraction analysis of whole rock was performed with the shale samples in this study. The major minerals for the shale samples including YC-L shale are divided into two types, one is clay minerals and the other is brittle minerals. **Table 5** shows the contents of clay minerals and brittle minerals for these shale samples. The contents of brittle minerals for NJZ, SHJ, MM, and YC-L shales are 57.3, 50.9, 28.7, and 60.0%, while those of clay minerals for the samples are 42.7, 49.1, 71.1, and 40.0%, respectively. The mineralogical data shows that MM oil shale has the lowest brittle mineral content but the highest clay mineral content, while the other shale samples have almost similar contents of brittle and clay minerals. A study by

TABLE 2 | Kinetic parameters obtained from Rock-Eval pyrolysis for grains and kerogen from NJZ shale, SHJ shale, and MM oil shale.

Sample	Form	E_a range (kcal/mol)	E_{max} (kcal/mol)	A (s^{-1})
Nenjiang	Grain	38–60	48	$A = 1.98 \times 10^{12} s^{-1}$
	Kerogen	38–59	48	
Shahejie	Grain	38–58	48	
	Kerogen	38–58	47	
Maoming	Grain	38–61	48	
	Kerogen	38–58	47	

A is a frequency factor; E_a is activation energy; E_{max} is the activation energy for maximum petroleum potential.

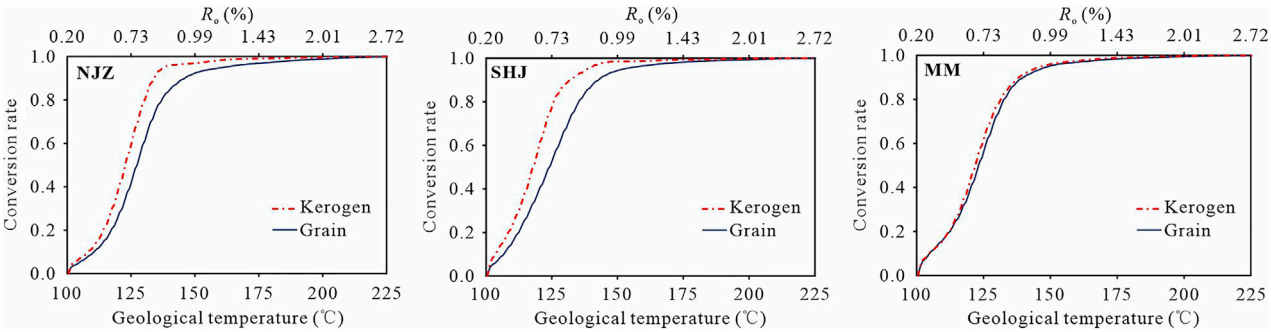

FIGURE 8 | Conversion rate versus geological temperature and maturity for three samples at a geological rate of 3°C/Ma.

TABLE 3 | Division of the main hydrocarbon generation period of three samples.

Sample	Form	Main hydrocarbon generation period	
		R_o (%)	T (°C)
NJZ	Grain	0.63–0.91	110–145
	Kerogen	0.61–0.80	108–134
SHJ	Grain	0.58–0.88	106–142
	Kerogen	0.54–0.77	103–131
MM	Grain	0.55–0.86	104–140
	Kerogen	0.55–0.84	104–138

The division of the main hydrocarbon generation period (MHGP) was explained in detail in Liao et al. (2018).

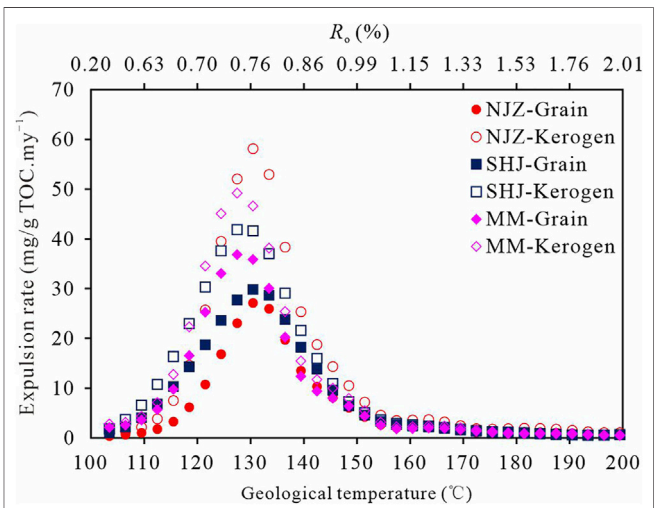

FIGURE 9 | Expulsion rates for three samples at a geological heating rate of 3°C/Ma.

Ross and Bustin, (2008) suggested that the content of clay minerals might affect the hydrocarbon expulsion of source rock. However, it is found that the retention content and retention proportion of MM oil shale with the highest abundance of clay minerals show a very slight difference compared with SHJ shale and YC-L shale having a relatively low abundance of clay minerals. It is worth noting that the retention content and retention proportion vary vastly among NJZ, SHJ, and YC-L shales, although there is little difference in the mineralogical compositions between them. This may suggest that mineralogical composition is not responsible for the hydrocarbon retention capacity for the shales in this study.

The reservoirs of NJZ shale are of ultra-low porosity and of ultra-low permeability (Wang, 2014). The porosity of NJZ shale is ranged from 3.67 to 5.15% with an average of 4.36%. The pore diameter is ranged from 1 to 3 μm (only a few of them reach 4–5 μm). The permeability is ranged from 0.00054×10^{-3} to 0.006515×10^{-3} μm^2. SHJ shale has a relatively larger pore diameter and higher permeability. The pore diameter for SHJ shale ranges from 44 to 250 nm with an average of 76 nm, the porosity from 0.5 to 9.8%, with an average of 5.6%, and the permeability from 0.06×10^{-3} to 1.60×10^{-3} μm^2 (Zou et al., 2011). The porosity of YC-L ranges from 0.5 to 3.5%, and about 70% of YC-L shale contains a permeability of less than 0.01×10^{-3} μm^2. The pore diameter typically ranges from 6 to 9 nm with

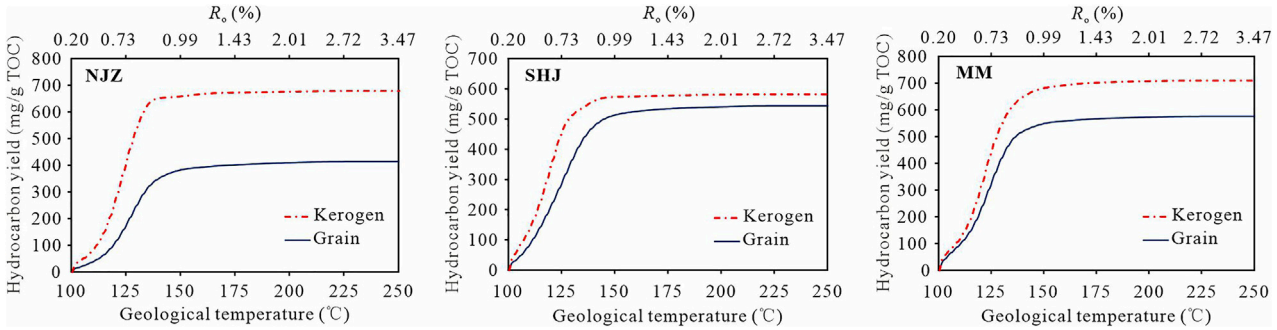

FIGURE 10 | Characteristics of hydrocarbon generation, retention, and expulsion for three samples at a geological heating rate of 3°C/Ma.

TABLE 4 | Amount of hydrocarbon generation, retention, and expulsion for three samples in stage I (R_o = 1%) and stage II (R_o = 3%).

Samples	Form	R_o = 1%			R_o = 3%		
		Hydrocarbon yield (mg/g TOC)	Retention (mg/g TOC)	Retention proportion (%)	Hydrocarbon yield (mg/g TOC)	Retention (mg/g TOC)	Retention proportion (%)
NJZ	Grain	384.71	274.94	41.68	414.08	264.82	39.01
	Kerogen	659.65	—	—	678.90	—	—
SHJ	Grain	515.61	57.97	10.11	543.97	38.03	6.53
	Kerogen	573.58	—	—	582.00	—	—
MM	Grain	551.08	132.42	19.37	576.30	133.26	18.78
	Kerogen	683.50	—	—	709.56	—	—
YC-L	Grain	338.59	66.92	16.50	375.09	70.66	15.85
	Kerogen	405.51	—	—	445.75	—	—

The data of YC-L were obtained from Liao et al. (2018).

TABLE 5 | Main mineral contents of four shale samples.

Sample	Brittle mineral		Clay mineral	
	Component	Proportion (%)	Component	Proportion (%)
NJZ	Quartz, calcite, and microcline	57.3	Illite and chlorite	42.7
SHJ	Quartz, calcite, and dolomite	50.9	Kaolinite and illite	49.1
MM	Quartz and pyrite	28.7	Kaolinite, montmorillonite, and illite	71.1
YC-L	Quartz, pyrite, microcline, and calcite	60.0	Illite, montmorillonite, kaolinite, and chlorite	40.0

an average of 7.2 nm (Gao et al., 2014; Dai et al., 2016), which belongs to ultra-low permeability and low porosity shale (Zeng et al., 2008). For MM oil shale, the pore size ranges from 0.35 to 200 nm (Gao et al., 2016), and the porosity ranges from 13 to 24% with an average of 17% (Li, 2016). The fissure of MM oil shale is barely developed due to less mechanical compaction/consolidation in the late stage of diagenesis (Li, 2016). At this stage, shales are immature even if they have high organic carbon contents. As a consequence, the MM oil shale exhibits a relatively weak hydrocarbon retention capacity. This may indicate that the discrepancy in hydrocarbon retention ability/capacity is mainly attributable to the pore structure (porosity and permeability) of lacustrine shales in China. The results also reveal that high pore diameter and permeability facilitate strong ability of hydrocarbon expulsion from the lacustrine shales, that is, SHJ shale has the highest pore diameter and permeability and the strongest hydrocarbon expulsion ability, whereas NJZ shale has the lowest pore size and permeability and the weakest hydrocarbon expulsion ability.

CONCLUSION

Overall, three sets of lacustrine shales from continental basins in China were investigated by a grain-based Rock-Eval pyrolysis method to reveal the evolution characteristics of hydrocarbon generation, expulsion, and retention of the shales. The pyrolysis and kinetic parameters showed that the Nenjiang shale has a relatively higher generation threshold than the Shahejie shale and Maoming oil shale while extrapolating to a geological heating rate of 3°C/Ma. Both the Shahejie shale and the Maoming oil shale need lower energy for hydrocarbon generation but higher energy

for hydrocarbon expulsion, while the Nenjiang shale requires higher energy for both processes.

By comparison of the pyrolysis results of shale grain and kerogen samples, the retention content and proportion of the shales were estimated approximately. The Nenjiang shale has the highest hydrocarbon retention content and retention proportion, followed by the Maoming oil shale, the Yanchang shale, and Shahejie shale. At the earlier maturation stage (R_o = 1%), the retention proportions for the Nenjiang, Shahejie, and Maoming shale samples were estimated as 41.68, 10.11, and 19.37% and then changed to 39.01, 6.53, and 18.78% at the advanced maturation stage (R_o = 3%), respectively. This indicates that the Nenjiang shale from the Songliao Basin has the strongest retention ability but the weakest expulsion ability, while the Shahejie shale from the Dongying Depression has the strongest hydrocarbon expulsion ability but the weakest hydrocarbon retention ability. Furthermore, the hydrocarbon retention capacity of lacustrine shales may largely depend on the pore structure (porosity and permeability) of the shales, rather than the compositions of the minerals and organic matter therein.

DATA AVAILABILITY STATEMENT

The original contributions presented in the study are included in the article/Supplementary Material; further inquiries can be directed to the corresponding author.

AUTHOR CONTRIBUTIONS

LL completed the experiments, acquired data, and drafted the manuscript; YW provided ideas and platforms for the experiments; CC processed samples; YP supervised and revised the manuscript.

FUNDINGS

This work was supported by the National Natural Science Foundation of China (Grant Nos. 41902152 and 41702151), and Strategic Priority Research Program of the Chinese Academy of Sciences (Grant No. XDA14010103).

REFERENCES

Badics, B., and Vető, I. (2012). Source Rocks and Petroleum Systems in the Hungarian Part of the Pannonian Basin: The Potential for Shale Gas and Shale Oil Plays. *Mar. Pet. Geol.* 31 (1), 53–69. doi:10.1016/j.marpetgeo.2011.08.015

Behar, F., Kressmann, S., Rudkiewicz, J., and Vandenbroucke, M. (1992). Experimental Simulation in a Confined System and Kinetic Modelling of Kerogen and Oil Cracking. *Org. Geochem.* 19 (1–3), 173–189. doi:10.1016/0146-6380(92)90035-V

Bowker, K. A. (2007). Barnett Shale Gas Production, Fort Worth Basin: Issues and Discussion. *Bulletin* 91 (4), 523–533. doi:10.1306/06190606018

Brassell, S. C., Eglinton, G., and Mo, F. J. (1986). Biological Marker Compounds as Indicators of the Depositions! History of the Maoming Oil Shale. *Org. Geochem.* 10 (4–6), 927–941. doi:10.1016/s0146-6380(86)80030-4

Chalmers, G. R. L., and Bustin, R. M. (2007). The Organic Matter Distribution and Methane Capacity of the Lower Cretaceous Strata of Northeastern British Columbia, Canada. *Int. J. Coal Geol.* 70 (1–3), 223–239. doi:10.1016/j.coal.2006.05.001

Chalmers, G. R. L., Ross, D. J. K., and Bustin, R. M. (2012). Geological Controls on Matrix Permeability of Devonian Gas Shales in the Horn River and Liard Basins, Northeastern British Columbia, Canada. *Int. J. Coal Geol.* 103, 120–131. doi:10.1016/j.coal.2012.05.006

Cheng, P., Tian, H., Xiao, X., Gai, H., Li, T., and Wang, X. (2017). Water Distribution in Overmature Organic-Rich Shales: Implications from Water Adsorption Experiments. *Energy Fuels.* 31, 13120–13132. doi:10.1021/acs.energyfuels.7b01531

Cheng, P., Xiao, X., Tian, H., and Wang, X. (2018). Water Content and Equilibrium Saturation and Their Influencing Factors of the Lower Paleozoic Overmature Organic-Rich Shales in the Upper Yangtze Region of Southern China. *Energy Fuels.* 32, 11452–11466. doi:10.1021/acs.energyfuels.8b03011

Cheng, P., Xiao, X., Wang, X., Sun, J., and Wei, Q. (2019). Evolution of Water Content in Organic-Rich Shales with Increasing Maturity and its Controlling Factors: Implications from a Pyrolysis Experiment on a Water-Saturated Shale Core Sample. *Mar. Pet. Geol.* 109, 291–303. doi:10.1016/j.marpetgeo.2019.06.023

Cheng, P., Xiao, X., Tian, H., Gai, H., Zhou, Q., Li, T., et al. (2022). Differences in the Distribution and Occurrence Phases of Pore Water in Various Nanopores of Marine-Terrestrial Transitional Shales in the Yangquan Area of the Northeast Qinshui Basin, China. *Mar. Pet. Geol.* 137, 105510. doi:10.1016/j.marpetgeo.2021.105510

Cornford, C., Gardner, P., and Burgess, C. (1998). Geochemical Truths in Large Data Sets. I: Geochemical Screening Data. *Org. Geochem.* 29 (1–3), 519–530. doi:10.1016/s0146-6380(98)00189-2

Dai, J., Zou, C., Dong, D., Ni, Y., Wu, W., Gong, D., et al. (2016). Geochemical Characteristics of Marine and Terrestrial Shale Gas in China. *Mar. Pet. Geol.* 76, 444–463. doi:10.1016/j.marpetgeo.2016.04.027

Espitalié, J., Laporte, J. L., Madec, M., Marquis, F., Leplat, P., Paulet, J., et al. (1977). Méthode rapide de caractérisation des roches mètres, de leur potentiel pétrolier et de leur degré d'évolution. *Rev. l'Institut français Pétrole* 32 (1), 23–42. doi:10.2516/ogst:1977002

Gao, L., Schimmelmann, A., Tang, Y., and Mastalerz, M. (2014). Isotope Rollover in Shale Gas Observed in Laboratory Pyrolysis Experiments: Insight to the Role of Water in Thermogenesis of Mature Gas. *Org. Geochem.* 68, 95–106. doi:10.1016/j.orggeochem.2014.01.010

Gao, Y., Long, Q., Su, J., He, J., and Guo, P. (2016). Approaches to Improving the Porosity and Permeability of Maoming Oil Shale, South China. *Oil shale* 33 (3), 216–227. doi:10.3176/oil.2016.3.02

Guo, H., Jia, W., Peng, P. a., Lei, Y., Luo, X., Cheng, M., et al. (2014). The Composition and its Impact on the Methane Sorption of Lacustrine Shales from the Upper Triassic Yanchang Formation, Ordos Basin, China. *Mar. Pet. Geol.* 57, 509–520. doi:10.1016/j.marpetgeo.2014.05.010

Han, S., Horsfield, B., Zhang, J., Chen, Q., Mahlstedt, N., di Primio, R., et al. (2014). Hydrocarbon Generation Kinetics of Lacustrine Yanchang Shale in Southeast Ordos Basin, North China. *Energy Fuels.* 28 (9), 5632–5639. doi:10.1021/ef501011b

Han, H., Guo, C., Zhong, N.-n., Pang, P., Chen, S.-j., Lu, J.-g., et al. (2019). Pore Structure Evolution of Lacustrine Shales Containing Type I Organic Matter from the Upper Cretaceous Qingshankou Formation, Songliao Basin, China: A Study of Artificial Samples from Hydrous Pyrolysis Experiments. *Mar. Pet. Geol.* 104, 375–388. doi:10.1016/j.marpetgeo.2019.04.001

Hanson, A. D., Ritts, B. D., and Moldowan, J. M. (2007). Organic Geochemistry of Oil and Source Rock Strata of the Ordos Basin, North-Central China. *Bulletin* 91 (9), 1273–1293. doi:10.1306/05040704131

Horsfield, B., and Schulz, H.-M. (2012). Shale Gas Exploration and Exploitation. *Mar. Pet. Geol.* 31 (1), 1–2. doi:10.1016/j.marpetgeo.2011.12.006

Hu, A., Li, J., Zhang, W., Li, Z., Hou, L., and Liu, Q. (2008). Geochemical Characteristics and Origin of Gases from the Upper, Lower Paleozoic and the Mesozoic Reservoirs in the Ordos Basin, China. *Sci. China Ser. D-Earth Sci.* 51, 183–194. doi:10.1007/s11430-008-5005-1

Inan, S., Yalcin, M. N., and Mann, U. (1998). Expulsion of Oil from Petroleum Source Rocks: Inferences from Pyrolysis of Samples of Unconventional Grain Size. *Org. Geochem.* 29 (1–3), 45–61. doi:10.1016/S0146-6380(98)00091-6

Jarvie, D. M., Hill, R. J., Ruble, T. E., and Pollastro, R. M. (2007). Unconventional Shale-Gas Systems: The Mississippian Barnett Shale of North-Central Texas as One Model for Thermogenic Shale-Gas Assessment. *Bulletin* 91 (4), 475–499. doi:10.1306/12190606068

Ji, W., Song, Y., Jiang, Z., Wang, X., Bai, Y., and Xing, J. (2014). Geological Controls and Estimation Algorithms of Lacustrine Shale Gas Adsorption Capacity: A Case Study of the Triassic Strata in the Southeastern Ordos Basin, China. *Int. J. Coal Geol.* 134-135, 61–73. doi:10.1016/j.coal.2014.09.005

Jia, C. Z. (2020). Development Challenges and Future Scientific and Technological Researches in China's Petroleum Industry Upstream. *Acta Pet. Sin.* 41 (12), 1445–1464. doi:10.7623/syxb202012001

Jin, Z. J., Wang, G,P., Liu, G. X., Gao, B., Liu, Q. Y., Wang, H. L., et al. (2021). Research Progress and Key Scientific Issues of Continental Shale Oil in China. *Acta Pet. Sin.* 42 (7), 821–835. doi:10.7623/syxb202107001

Lamei, L., Zhang, J. C., Tang, X., Jing, T. Y., and Zhu, L. L. (2013). Conditions of Continental Shale Gas Accumulation in China. *Nat. Gas. Ind.* 33 (1), 35–40. doi:10.3787/j.issn.1000-0976.2013.01.005

Li, X., Liu, X., Zhou, S., Liu, H., Chen, Q., Wang, J., et al. (2012). Hydrocarbon Origin and Reservoir Forming Model of the Lower Yanchang Formation, Ordos Basin. *Pet. Explor. Dev.* 39 (2), 184–193. doi:10.1016/S1876-3804(12)60031-7

Li, A., Ding, W., He, J., Dai, P., Yin, S., and Xie, F. (2016). Investigation of Pore Structure and Fractal Characteristics of Organic-Rich Shale Reservoirs: A Case Study of Lower Cambrian Qiongzhusi Formation in Malong Block of Eastern Yunnan Province, South China. *Mar. Pet. Geol.* 70, 46–57. doi:10.1016/j.marpetgeo.2015.11.004

Li, W., Cao, J., Shi, C., Xu, T., Zhang, H., and Zhang, Y. (2020). Shale Oil in Saline Lacustrine Systems: A Perspective of Complex Lithologies of Fine-Grained Rocks. *Mar. Pet. Geol.* 116, 104351. doi:10.1016/j.marpetgeo.2020.104351

Li, W., Cao, J., Zhi, D., Tang, Y., He, W., Wang, T., et al. (2021). Controls on Shale Oil Accumulation in Alkaline Lacustrine Settings: Late Paleozoic Fengcheng Formation, Northwestern Junggar Basin. *Mar. Pet. Geol.* 129, 105107. doi:10.1016/j.marpetgeo.2021.105107

Li, Q., Chen, F., Wu, S., Zhang, L., Wang, Y., and Xu, S. (2022). A Simple and Effective Evaluation Method for Lacustrine Shale Oil Based on Mass Balance Calculation of Rock-Eval Data. *Appl. Geochem.* 140, 105287. doi:10.1016/j.apgeochem.2022.105287

Li, P. (2016). *Reservoir Characteristics of the Youganwo Formation Shale in Maoming Basin of Guangdong Province*. Xuzhou: China University of Mining and Technology, 1–89.

Liao, L., Wang, Y., and Lu, J. (2016). Evaluation of Residual Oil Content, Composition, and Evolution of Marine Shale from the Middle Ordovician Pingliang Formation, Erdos Basin, China. *Pet. Sci. Technol.* 34 (7), 671–676. doi:10.1080/10916466.2016.1157604

Liao, L., Wang, Y., Chen, C., Shi, S., and Deng, R. (2018). Kinetic Study of Marine and Lacustrine Shale Grains Using Rock-Eval Pyrolysis: Implications to Hydrocarbon Generation, Retention and Expulsion. *Mar. Pet. Geol.* 89 (1), 164–173. doi:10.1016/j.marpetgeo.2017.01.009

Liu, L. Q., Li, Y., Kang, L. M., Li, B., and Zou, H. (2010). Mudstone Distribution Features of Maximum Flooding Time in Late Triassic in Ordos Basin [J]. *J. Northwest Univ. Nat. Sci. Ed.* 40 (5), 866–871. doi:10.16152/j.cnki.xdxbzr.2010.05.016

Loucks, R. G., Reed, R. M., Ruppel, S. C., and Hammes, U. (2012). Spectrum of Pore Types and Networks in Mudrocks and a Descriptive Classification for Matrix-Related Mudrock Pores. *Bulletin* 96 (6), 1071–1098. doi:10.1306/08171111061

Ma, Y., Zhong, N., Li, D., Pan, Z., Cheng, L., and Liu, K. (2015). Organic Matter/clay Mineral Intergranular Pores in the Lower Cambrian Lujiaping Shale in the North-Eastern Part of the Upper Yangtze Area, China: A Possible Microscopic Mechanism for Gas Preservation. *Int. J. Coal Geol.* 137, 38–54. doi:10.1016/j.coal.2014.11.001

Mastalerz, M., He, L., Melnichenko, Y. B., and Rupp, J. A. (2012). Porosity of Coal and Shale: Insights from Gas Adsorption and SANS/USANS Techniques. *Energy Fuels.* 26 (8), 5109–5120. doi:10.1021/ef300735t

Miura, K. (1995). A New and Simple Method to Estimate F (E) and K0 (E) in the Distributed Activation Energy Model from Three Sets of Experimental Data. *Energy Fuels.* 9 (2), 302–307. doi:10.1021/ef00050a014

Mukhopadhyay, P. K., Wade, J. A., and Kruge, M. A. (1995). Organic Facies and Maturation of Jurassic/Cretaceous Rocks, and Possible Oil-Source Rock Correlation Based on Pyrolysis of Asphaltenes, Scotian Basin, Canada. *Org. Geochem.* 22, 85–104. doi:10.1016/0146-6380(95)90010-1

Peng, P. A., and Jia, C. Z. (2021). Evolution of Deep Source Rock and Resource Potential of Primary Light Oil and Condensate. *Acta Pet. Sin.* 42 (12), 1543–1555. doi:10.7623/syxb202112001

Peters, K. E., and Cassa, M. R. (1994). Applied Source Rock Geochemistry: Chapter 5: Part II. Essential Elements. *Gelolgy*.

Ross, D. J. K., and Bustin, R. M. (2008). Characterizing the Shale Gas Resource Potential of Devonian-Mississippian Strata in the Western Canada Sedimentary Basin: Application of an Integrated Formation Evaluation. *Bulletin* 92 (1), 87–125. doi:10.1306/09040707048

Ross, D. J. K., and Marc Bustin, R. (2009). The Importance of Shale Composition and Pore Structure upon Gas Storage Potential of Shale Gas Reservoirs. *Mar. Pet. Geol.* 26 (6), 916–927. doi:10.1016/j.marpetgeo.2008.06.004

Schenk, H. J., Di Primio, R., and Horsfield, B. (1997). The Conversion of Oil into Gas in Petroleum Reservoirs. Part 1: Comparative Kinetic Investigation of Gas Generation from Crude Oils of Lacutrine, Marine and Fluviodeltaic Origin by Programmed-Temperature Closed-System Pyrolysis. *Org. Geochem.* 26 (7–8), 467–481. doi:10.1016/S0146-6380(97)00024-7

Shalaby, M. R., Hakimi, M. H., and Abdullah, W. H. (2011). Geochemical Characteristics and Hydrocarbon Generation Modeling of the Jurassic Source Rocks in the Shoushan Basin, North Western Desert, Egypt. *Mar. Pet. Geol.* 28 (9), 1611–1624. doi:10.1016/j.marpetgeo.2011.07.003

Tang, X., Zhang, J., Wang, X., Yu, B., Ding, W., Xiong, J., et al. (2014). Shale Characteristics in the Southeastern Ordos Basin, China: Implications for Hydrocarbon Accumulation Conditions and the Potential of Continental Shales. *Int. J. Coal Geol.* 128-129, 32–46. doi:10.1016/j.coal.2014.03.005

Wang, Y., Zhang, S., Wang, F., Wang, Z., Zhao, C., Wang, H., et al. (2006). Thermal Cracking History by Laboratory Kinetic Simulation of Paleozoic Oil in Eastern Tarim Basin, NW China, Implications for the Occurrence of Residual Oil Reservoirs. *Org. Geochem.* 37 (12), 1803–1815. doi:10.1016/j.orggeochem.2006.07.010

Wang, Q., Chen, X., Jha, A. N., and Rogers, H. (2014). Natural Gas from Shale Formation - the Evolution, Evidences and Challenges of Shale Gas Revolution in United States. *Renew. Sustain. Energy Rev.* 30, 1–28. doi:10.1016/j.rser.2013.08.065

Wang, M., Wilkins, R. W. T., Song, G., Zhang, L., Xu, X., Li, Z., et al. (2015). Geochemical and Geological Characteristics of the Es3L Lacustrine Shale in the Bonan Sag, Bohai Bay Basin, China. *Int. J. Coal Geol.* 138, 16–29. doi:10.1016/j.coal.2014.12.007

Wang, M., Guo, Z., Jiao, C., Lu, S., Li, J., Xue, H., et al. (2019). Exploration Progress and Geochemical Features of Lacustrine Shale Oils in China. *J. Pet. Sci. Eng.* 178, 975–986. doi:10.1016/j.petrol.2019.04.029

Wang, M., Li, M., Li, J.-B., Xu, L., Zhang, J.-Y., and Zhang, J.-X. (2022). The Key Parameter of Shale Oil Resource Evaluation: Oil Content. *Pet. Sci.* In press. doi:10.1016/j.petsci.2022.03.006

Wang, M. (2014). *The Generation and Potential of Shale Oil for N1 and N2 Interval in Northern Songliao Basin*. Daqing: Northeast Petroleum University, 1–71.

Xie, X., Li, M., Littke, R., Huang, Z., Ma, X., Jiang, Q., et al. (2016). Petrographic and Geochemical Characterization of Microfacies in a Lacustrine Shale Oil System in the Dongying Sag, Jiyang Depression, Bohai Bay Basin, Eastern China. *Int. J. Coal Geol.* 165, 49–63. doi:10.1016/j.coal.2016.07.004

Xiong, J., Liu, X., and Liang, L. (2015). Experimental Study on the Pore Structure Characteristics of the Upper Ordovician Wufeng Formation Shale in the Southwest Portion of the Sichuan Basin, China. *J. Nat. Gas Sci. Eng.* 22, 530–539. doi:10.1016/j.jngse.2015.01.004

Yang, Y., Li, W., and Ma, L. (2005). Tectonic and Stratigraphic Controls of Hydrocarbon Systems in the Ordos Basin: A Multicycle Cratonic Basin in Central China. *Bulletin* 89 (2), 255–269. doi:10.1306/10070404027

Yu, Y., Luo, X., Cheng, M., Lei, Y., Wang, X., Zhang, L., et al. (2017). Study on the Distribution of Extractable Organic Matter in Pores of Lacustrine Shale: An Example of Zhangjiatan Shale from the Upper Triassic Yanchang Formation, Ordos Basin, China. *Interpretation* 5 (2), SF109–SF126. doi:10.1190/int-2016-0124.1

Zeng, L., Gao, C., Qi, J., Wang, Y., Li, L., and Qu, X. (2008). The Distribution Rule and Seepage Effect of the Fractures in the Ultra-low Permeability Sandstone

Reservoir in East Gansu Province, Ordos Basin. *Sci. China Ser. D-Earth Sci.* 51, 44–52. doi:10.1007/s11430-008-6015-8

Zhang, J., Li, X., Wei, Q., Sun, K., Zhang, G., and Wang, F. (2017a). Characterization of Full-Sized Pore Structure and Fractal Characteristics of Marine-Continental Transitional Longtan Formation Shale of Sichuan Basin, South China. *Energy Fuels.* 31 (10), 10490–10504. doi:10.1021/acs.energyfuels.7b01456

Zhang, J., Li, X., Wei, Q., Gao, W., Liang, W., Wang, Z., et al. (2017b). Quantitative Characterization of Pore-Fracture System of Organic-Rich Marine-Continental Shale Reservoirs: A Case Study of the Upper Permian Longtan Formation, Southern Sichuan Basin, China. *Fuel* 200, 272–281. doi:10.1016/j.fuel.2017.03.080

Zou, C., Dong, D., Wang, S., Li, J., Li, X., Wang, Y., et al. (2010). Geological Characteristics and Resource Potential of Shale Gas in China. *Pet. Explor. Dev.* 37 (6), 641–653. doi:10.1016/S1876-3804(11)60001-3

Zou, C. N., Dong, D. Z., Yang, H., Wang, Y. M., Huang, J. L., Wang, S. F., et al. (2011). Conditions of Shale Gas Accumulation and Exploration Practices in China. *Nat. Gas. Ind.* 31 (12), 26–39. doi:10.3787/j.issn.1000-0976.2011.12.005

Conflict of Interest: The authors declare that the research was conducted in the absence of any commercial or financial relationships that could be construed as a potential conflict of interest.